Fall Speeds and Masses of Solid Precipitation Particles

JOHN D. LOCATELLI AND PETER V. HOBBS

Cloud Physics Group, Atmospheric Sciences Department, University of Washington, Seattle, Washington 98195

Measurements have been made of the fall speeds and masses of a large number of different types of solid precipitation particles. Particular attention is paid to the effects of riming and aggregation on the fall speeds and masses. Empirical expressions are given for the relationships between fall speeds and maximum dimensions and between masses and maximum dimensions for the particles studied. The results are compared with other experimental observations when they exist.

The rate of increase in the mass of an ice particle due to collisions with supercooled cloud droplets (riming) and other ice particles (aggregation) as it moves through a cloud is dependent on its mass, dimensions, and fall speed. Also, in a given wind field the trajectory of a particle is determined by its fall speed, and the contribution that it makes to the precipitation rate is proportional to the product of its mass and fall speed. Consequently, as theoretical models of cloud and precipitation processes have become more refined, the need has increased for more detailed measurements of the relationships between the fall speeds, masses, and dimensions of various types of solid precipitation particles.

Although several sets of measurements of the fall speeds and masses of solid precipitation particles of various types and sizes have been reported [e.g., *Nakaya and Terada,* 1935; *Magono,* 1951, 1954; *Langleben,* 1954; *Litvinov,* 1956; *Bashkirova and Pershina,* 1964; *Brown,* 1970; *Zikmunda,* 1972; *Zikmunda and Vali,* 1972], the available data are still scanty and inadequate for many purposes. Moreover, some of the previous measurements show inconsistencies, and a complete pattern to the results has not emerged. This lack of pattern is not surprising in view of the fact that *Magono and Lee* [1966] classify snow crystals into 80 different types, and each of these types may exist over a wide range of sizes and with various degrees of riming and aggregation.

In this paper we present the results of a new set of measurements of the fall speeds and masses of a wide variety of solid precipitation particles obtained during the winter months of 1971–1972 and 1972–1973 in the Cascade Mountains of Washington. The effects of size, riming, aggregation, and density on the fall speeds and masses of different types of solid precipitation particles are considered.

INSTRUMENTATION AND PROCEDURES

The instrument used for measuring the fall speeds of solid precipitation particles is shown in Figure 1. The light sources consist of two incandescent lamps (18 W each), transmitted by fiber optics as two parallel beams of light separated by 4.1 cm. These two light beams are received by a similar set of fiber optics on the other side of the instrument, and the intensity of the two signals is recorded with two photomultiplier tubes. Decreases in the intensities of the beams caused by the fall of a precipitation particle through them are detected by the photomultiplier tubes and can be displayed on a storage oscilloscope. The time difference between the changes in intensity of the upper beam and those changes in the lower beam is

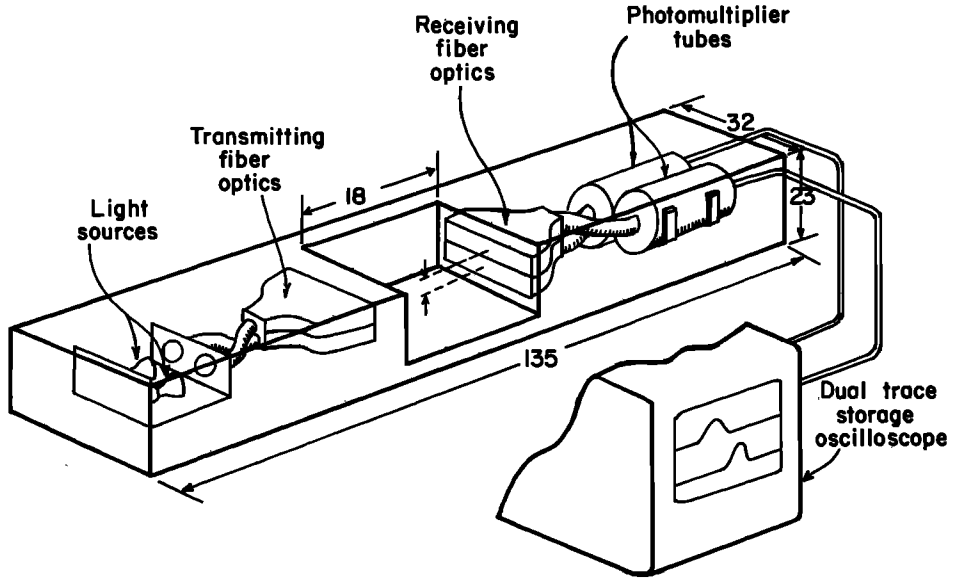

Fig. 1. Instrument for measuring fall speeds of solid precipitation particles. Dimensions are in centimeters.

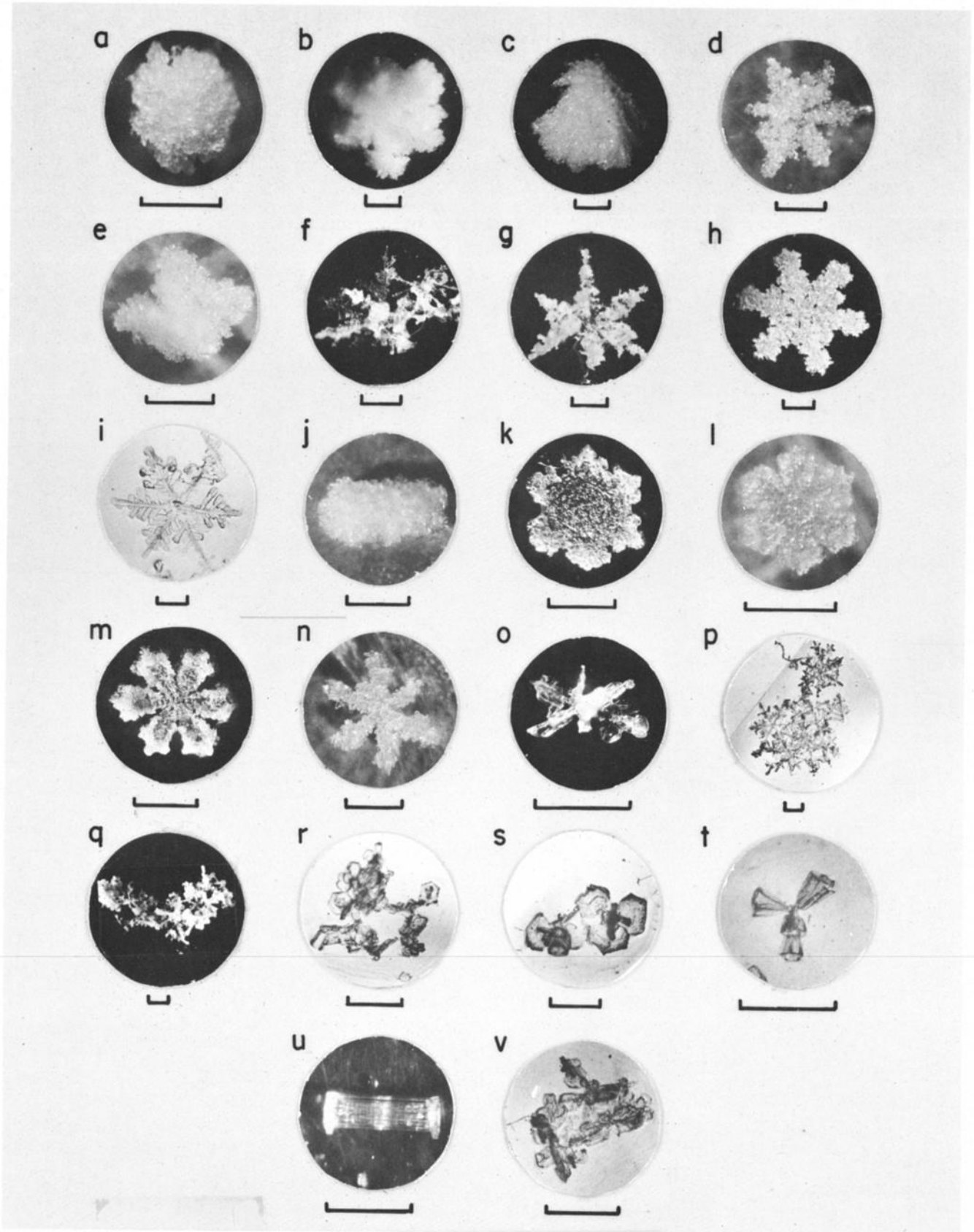
a
b
c
d
e
f
g
h
i
j
k
l
m
n
o
p
q
r
s
t
u
v

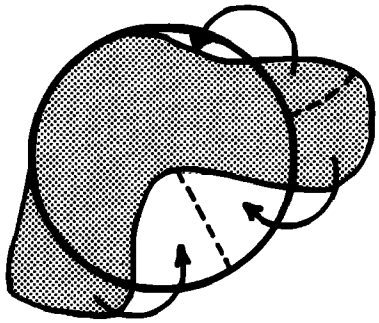

Fig. 3. Method of mental reassembly of a plane view of an aggregated snow crystal (shown shaded) into an equivalent circle.

recorded and is used to determine the fall speed of the particle. Since in no case was the size of the particle more than half the separation between the beams, two similarly shaped signals separated in time were observed on the storage oscilloscope. The time difference between the two signals was taken to be that between their peak values.

This instrument was located at the bottom of a tower 1.27 m square and 3.8 m high. After passing through the open upper end of this tower, precipitation particles were protected from the wind and fell vertically through the two light beams. Individual solid precipitation particles that passed through the light beams were caught on a thin sheet of plastic (Handiwrap, manufactured by Dow Chemical Company) stretched across a wooden frame. This plastic sheet minimized the shattering and bouncing of the ice particles on impact. Since the plastic sheet tended to give without springing back after the impact of the particle, even large graupel particles could be caught in this way. Some large aggregates did break up on collection, but these were ignored. The dimensions given for aggregates are probably somewhat larger than their free fall dimensions, since the aggregates tended to flatten on collection. Most observers measure the dimensions of aggregates after collection. The apparatus was fitted with inlet holes of various sizes, so that some adjustment of the flux of particles through the beams could be made. Even so, two or more particles would frequently pass through the beams simultaneously and would have to be ignored. Also, only those particles that landed on the plastic sheet at almost the same instant as the signals appeared on the oscilloscope were counted. These stringent precautions often necessitated many hours of observations to obtain a few reliable measurements.

After collection the ice particles were kept below 0°C by a thermoelectric module and maneuvered under a microscope in order to take microphotographs. These photographs were used to identify the dimensions of the particle in postanalysis. However, the particle was classified according to type by direct viewing through a stereomicroscope. The particle was subsequently melted, and a photograph was taken of the water drop into which it formed. The mass of the snow particle was determined from the diameter of the drop (drops in the case of aggregates) into which it melted. Since the drops were not perfectly spherical, a calibration curve was constructed for determining the masses of drops of various diameters when they were resting on the plastic sheet. The calibration curve was constructed by first making ice spheres of various sizes. These were then set on the plastic sheet and

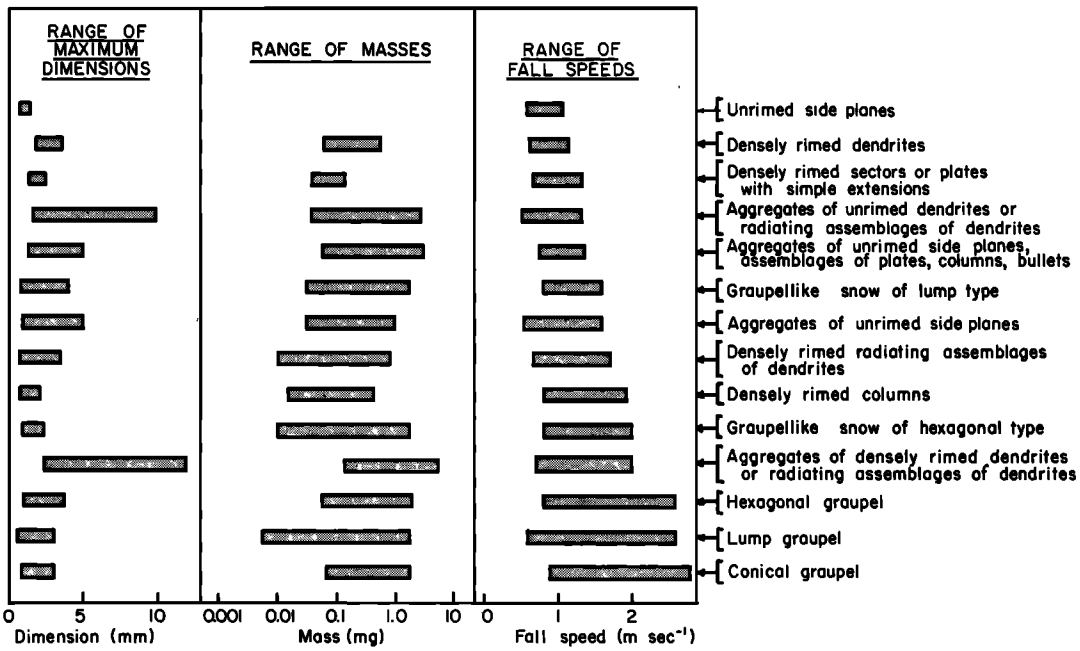

Fig. 4. Ranges of maximum dimensions, masses, and fall speeds of the solid precipitation particles observed in the present study.

Fig. 2. Types of solid precipitation particles on which measurements were made. (*a*) Lump graupel, (*b*) hexagonal graupel, (*c*) conical graupel, (*d*) graupellike snow of hexagonal type, (*e*) graupellike snow of lump type, (*f*) unrimed radiating assemblage of dendrites, (*g*) densely rimed radiating assemblage of dendrites, (*h*) densely rimed dendrite, (*i*) unrimed dendrite, (*j*) densely rimed column, (*k*) densely rimed plate with simple extensions, (*l*) densely rimed crystal with sectorlike branches, (*m*) densely rimed crystal with broad branches, (*n*) densely rimed stellar, (*o*) unrimed side plane, (*p*) lightly rimed aggregate of dendrites, (*q*) densely rimed aggregate of radiating assemblages of dendrites, (*r*) unrimed aggregate of bullets, columns, assemblages of plates, and side planes, (*s*) lightly rimed assemblage of plates, (*t*) unrimed bullets, (*u*) unrimed column, and (*v*) unrimed aggregate of side planes. The scaled line below each photograph represents 1 mm.

TABLE 1. Derived Relationships Between Fall Speeds, Masses, and Maximum Dimensions for Solid Precipitation Particles

Particle Type	Velocity-Size Relationship	Velocity-Mass Relationship	Mass-Size Relationship	Density Range, Mg m^{-3}	Range of Maximum Dimensions, mm
Lump graupel	$V = 1.16D^{0.46}$, $N = 35$, $r = 0.55$	$V = 1.3M^{0.15}$, $N = 35$, $r = 0.53$	$M = 0.042D^{3.0}$ $N = 35$, $r = 0.98$	0.05 to 0.1	0.5 to 2.0
Lump graupel	$V = 1.3D^{0.66}$, $N = 58$, $r = 0.77$	$V = 2.4M^{0.24}$, $N = 58$, $r = 0.84$	$M = 0.078D^{2.8}$, $N = 58$, $r = 0.93$	>0.1 to 0.20	0.5 to 3.0
Lump graupel	$V = 1.5D^{0.37}$, $N = 17$, $r = 0.58$	$V = 1.8M^{0.12}$, $N = 17$, $r = 0.52$	$M = 0.14D^{2.7}$, $N = 17$, $r = 0.98$	>0.2 to 0.45	0.5 to 1.0
Conical graupel	$V = 1.2D^{0.65}$, $N = 30$, $r = 0.70$	$V = 2.5M^{0.28}$, $N = 26$, $r = 0.81$	$M = 0.073D^{2.6}$, $N = 26$, $r = 0.91$	...	0.8 to 3.0
Hexagonal graupel	$V = 1.1D^{0.57}$, $N = 33$, $r = 0.77$	$V = 2.0M^{0.18}$, $N = 31$, $r = 0.76$	$M = 0.044D^{2.9}$, $N = 31$, $r = 0.93$	...	0.8 to 3.2
Graupellike snow of lump type*	$V = 1.1D^{0.28}$, $N = 17$, $r = 0.46$	$V = 1.4M^{0.08}$, $N = 17$, $r = 0.32$	$M = 0.059D^{2.1}$, $N = 17$, $r = 0.91$	...	0.5 to 2.2
Graupellike snow of hexagonal type†	$V = 0.86D^{0.25}$, $N = 22$, $r = 0.38$	$V = 1.4M^{0.14}$, $N = 22$, $r = 0.71$	$M = 0.021D^{2.4}$, $N = 22$, $r = 0.72$	...	0.8 to 2.8
Densely rimed columns	$V = 1.1L^{0.56}$, $N = 13$, $r = 0.79$	$V = 1.8M^{0.11}$, $N = 13$, $r = 0.49$	$M = 0.033L^{2.3}$, $N = 13$, $r = 0.78$	0.02 to 0.27	0.8 to 2.0
Densely rimed dendrites†	$V = 0.62D^{0.33}$, $N = 10$, $r = 0.54$	$V = 1.2M^{0.16}$, $N = 9$, $r = 0.68$	$M = 0.015D^{2.3}$, $N = 9$, $r = 0.90$	...	1.8 to 4.0
Densely rimed radiating assemblages of dendrites*	$V = 1.1D^{0.12}$, $N = 14$, $r = 0.23$	$V = 1.3M^{0.08}$, $N = 13$, $r = 0.34$	$M = 0.039D^{2.1}$, $N = 13$, $r = 0.92$	...	0.8 to 2.8
Unrimed side planes	$V = 0.81D^{0.99}$, $N = 10$, $r = 0.77$	...	...	...	0.4 to 1.2
Aggregates of unrimed radiating assemblages of dendrites or dendrites*	$V = 0.8D^{0.16}$, $N = 28$, $r = 0.20$	$V = 1.1M^{0.08}$, $N = 27$, $r = 0.15$	$M = 0.073D^{1.4}$, $N = 27$, $r = 0.91$	...	2.0 to 10.0
Aggregates of densely rimed radiating assemblages of dendrites or dendrites	$V = 0.79D^{0.27}$, $N = 27$, $r = 0.55$	$V = 1.3M^{0.15}$, $N = 25$, $r = 0.69$	$M = 0.037D^{1.9}$, $N = 25$, $r = 0.88$	...	2.0 to 12.0
Aggregates of unrimed radiating assemblages of plates, side planes, bullets, and columns§	$V = 0.69D^{0.41}$, $N = 31$, $r = 0.91$	$V = 1.2M^{0.07}$, $N = 19$, $r = 0.36$	$M = 0.037D^{1.9}$, $N = 19$, $r = 0.84$	...	For V vs. D, 0.2 to 3.0; for V vs. M and M vs. D, 1.0 to 3.0
Aggregates of unrimed side planes†	$V = 0.82D^{0.12}$, $N = 23$, $r = 0.29$	$V = 1.2M^{0.14}$, $N = 21$, $r = 0.63$	$M = 0.04D^{1.4}$, $N = 21$, $r = 0.78$	...	0.5 to 4.0

See text for definitions of maximum dimensions in ambiguous cases. Fall speed V is given in meters per second; mass M, in milligrams; and maximum dimension D or L, in millimeters; N is the number of datum points, and r is the correlation coefficient for the relationship.

*The probability that the correlation between V and D or V and M will be accidental is greater than 0.1.

†The probability that the correlation between V and D will be accidental is greater than 0.1.

§The probability that the correlation between V and M will be accidental is greater than 0.1.

allowed to melt. The diameter of the drop produced was measured, and then the drop was refrozen on the plastic sheet. The refrozen drop was then placed in oil and melted again, and its true spherical diameter was measured to deduce its mass. A calibration curve relating the diameters of the drops on the plastic sheet to their true masses was then constructed.

Particles were classified according to the scheme suggested by *Magono and Lee* [1966]. Photographs illustrating the types of particles referred to in this paper are shown in Figure 2. The maximum dimensions of the more irregular solid precipitation particles were defined as follows: conical graupel, the diameter of the blunt end (obviously, cone graupel is a special case, since the diameter of the blunt end is not always the maximum dimension; however, this is the dimension that most clearly defines the cross-sectional area of the particle perpendicular to the direction of fall and is therefore most appropriate to correlate with fall speed); branched particles (dendrites, hexagonal graupel, etc.), the average value of the length of the branches; and aggregates, the diameter of the smallest circle into which the aggregate as photographed will fit without changing its density (Figure 3).

In the cases in which sufficient data are available on a particular type of particle, an expression of the form $y = ax^b$ is fitted to the experimental observations of fall speeds and masses, masses and maximum dimensions, and fall speeds and maximum dimensions. The constants a and b are determined by rectifying the data through logarithmic conversions, and the correlation coefficients apply to the best-fit curves derived by this method. All our measurements were made between altitudes of 750 and 1500 m above sea level. The fall speeds are recorded as measured, since the difference in the fall speeds at these two levels amounts to only 4%. However, when previously published data are shown for comparison or used in computations, they are corrected to the average altitude at which our measurements were made.

Some General Features of the Measurements

The range of the maximum dimensions, masses, and fall speeds of the various solid precipitation particles observed in this study are shown in Figure 4. All the fall speeds measured by us fall in the range 0.5–3.0 m s^{-1}, unrimed side planes having the lowest speed and graupel having the highest.

Empirical relationships based on our measurements be-

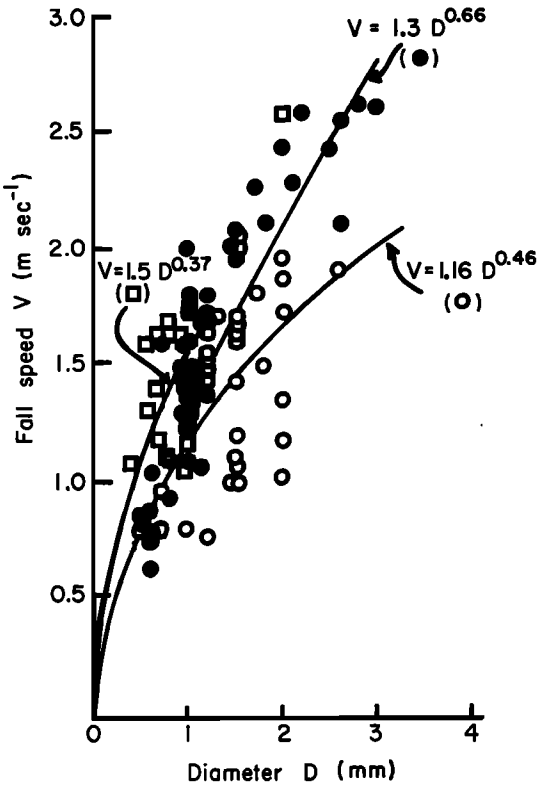

Fig. 5. Fall speeds versus diameters for lump graupel of three different density ranges: open circles, 0.05–0.1 Mg m^{-3}; solid circles, 0.1–0.2 Mg m^{-3}; and squares, 0.2–0.45 Mg m^{-3}.

tween the fall speeds V in meters per second, masses M in milligrams, and maximum dimensions D in millimeters of various types of precipitation particles are listed in Table 1. Cases for which the correlation coefficients for the derived relationships are low generally indicate real variations in the types of particle included in a given category rather than experimental errors. Thus lump graupel with densities between 0.1 and 0.2 Mg m^{-3} has correlation coefficients between 0.77 and 0.93, whereas graupellike snow of hexagonal type (densities not specified) has correlation coefficients from 0.38 to 0.72.

The detailed results shown in Table 1 can be summarized by the following approximate relationships. For graupel, $V \sim D^{0.6}$, $M \sim D^3$, and $V \sim M^{0.2}$; for densely rimed columns, dendrites, or radiating assemblages of dendrites, $V \sim D^{0.2}$, $M \sim D^2$, and $V \sim M^{0.1}$; for densely rimed aggregates, $V \sim D^{0.3}$, $M \sim D^2$, and $V \sim M^{0.2}$; and for unrimed aggregates, $V \sim D^{0.2}$, $M \sim D^2$, and $V \sim M^{0.1}$. *Langleben* [1954] found that the fall speeds of aggregated snowflakes varied as $M^{0.1}$. Our more detailed data show that this is approximately correct for un-

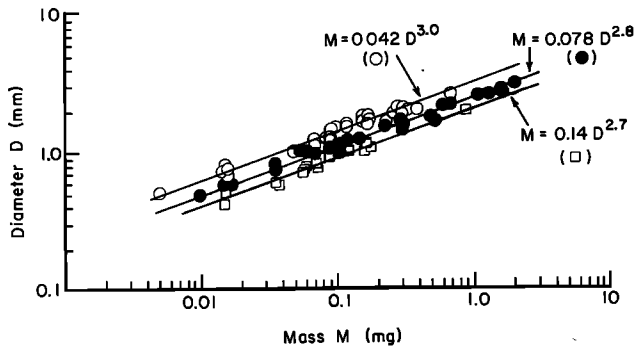

Fig. 6. Diameters versus masses for lump graupel of three different density ranges: open circles, 0.05–0.1 Mg m^{-3}; solid circles, 0.1–0.2 Mg m^{-3}; and squares, 0.2–0.45 Mg m^{-3}.

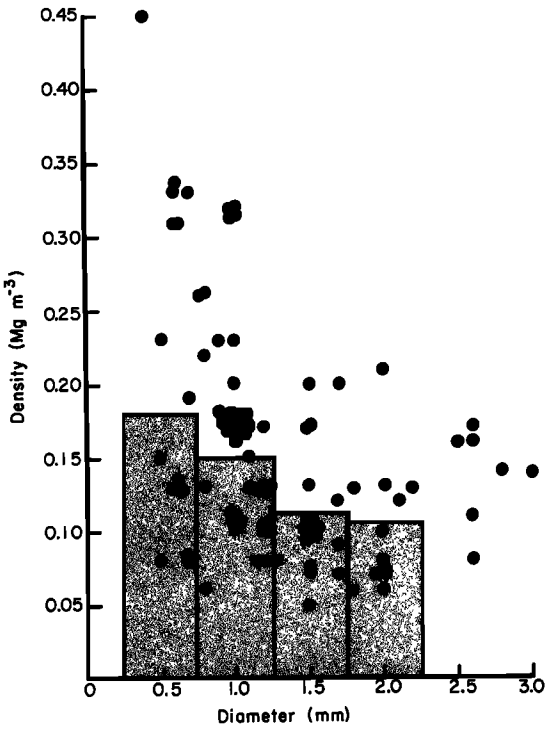

Fig. 7. Density versus diameter for lump graupel. The height of the shaded region is the average density of the lump graupel in the given diameter range.

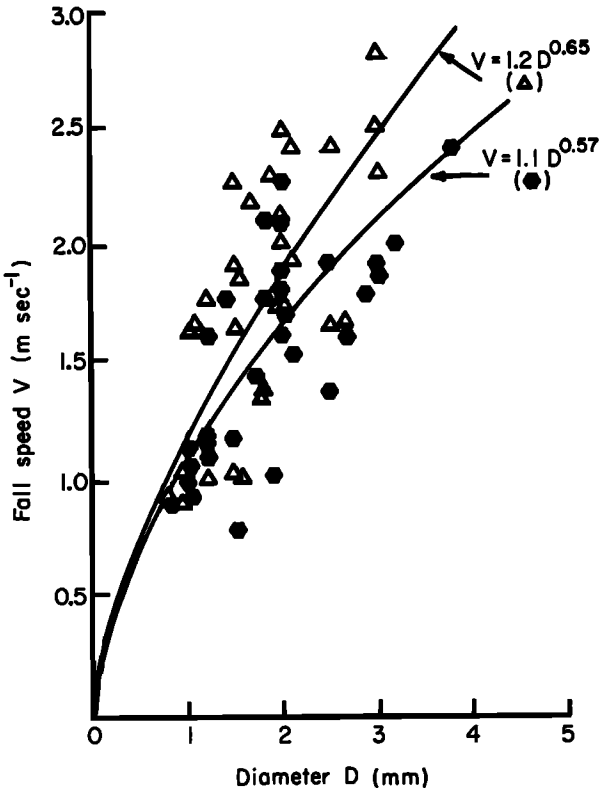

Fig. 8. Fall speeds versus diameters for conical graupel (triangles) and hexagonal graupel (hexagons).

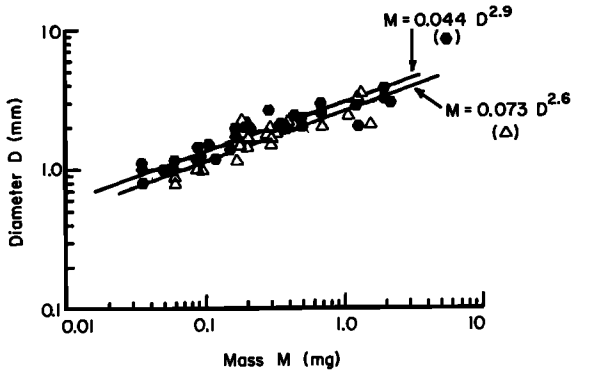

Fig. 9. Diameters versus masses for conical graupel (triangles) and hexagonal graupel (hexagons).

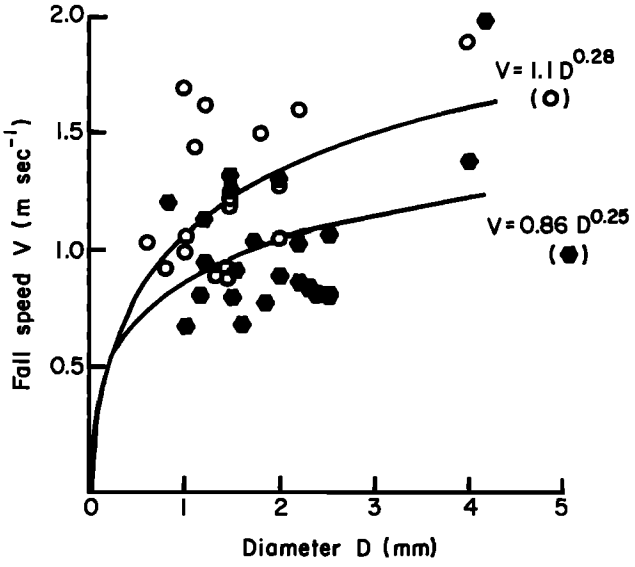

Fig. 10. Fall speeds versus diameters for graupellike snow of lump type (circles) and hexagonal type (hexagons).

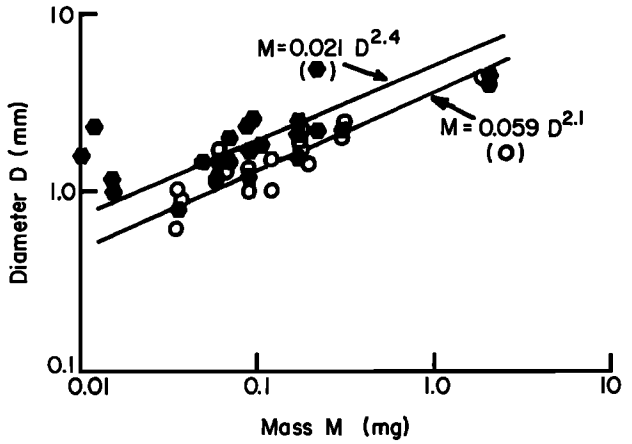

Fig. 11. Diameters versus masses for graupellike snow of lump type (circles) and hexagonal type (hexagons).

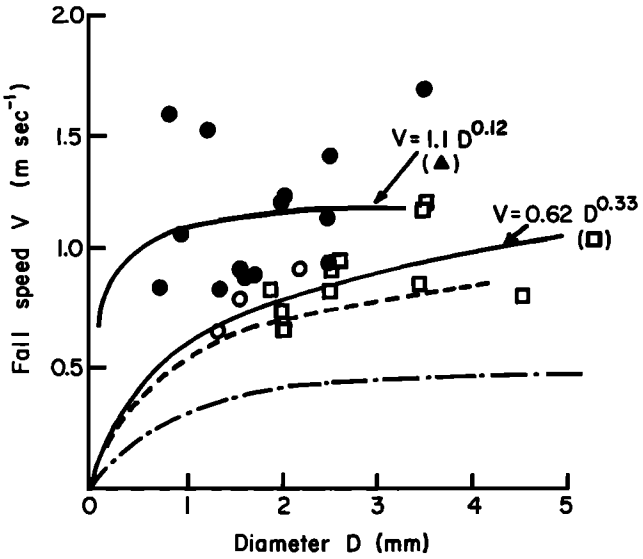

Fig. 12. Fall speeds versus diameters for unrimed radiating assemblages of dendrites (open circles), densely rimed radiating assemblages of dendrites (solid circles), and densely rimed dendrites (squares). The empirical relationship (broken line) for unrimed radiating assemblages of dendrites is from *Zikmunda and Vali* [1972]. The empirical relationship (dash-dot line) for unrimed dendrites is from *Brown* [1970].

rimed aggregates, but for densely rimed aggregates, $V \sim M^{0.2}$. The higher power for the rimed aggregates is presumably due to the fact that riming increases the mass of an aggregate much more rapidly than it increases its size or the drag force.

In the following sections we present our experimental data in more detail and when it is possible compare them with previous observations.

SINGLE SOLID PRECIPITATION PARTICLES

Lump graupel (Figure 2a). For lump graupel, which is approximately spherical, densities could be calculated. By dividing the data into three density ranges, namely, 0.05–0.10, 0.10–0.20, and 0.20–0.45 Mg m^{-3}, it was found that the results showed less scatter than they would have if density were ignored.

The measurements of the fall speeds of lump graupel of various diameters are shown in Figure 5. It can be seen that

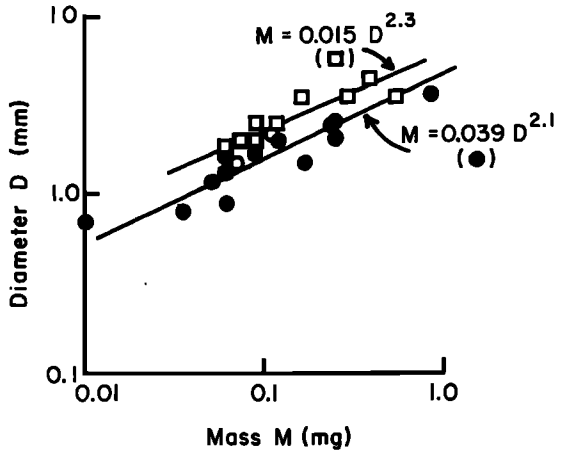

Fig. 13. Diameters versus masses for unrimed radiating assemblages of dendrites (open circles), densely rimed radiating assemblages of dendrites (solid circles), and densely rimed dendrites (squares).

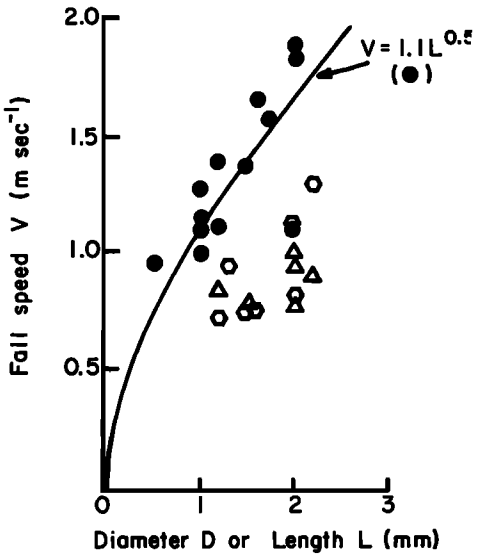

Fig. 14. Fall speeds versus diameters or lengths for densely rimed columns (circles), densely rimed stellars and crystals with broad branches (triangles), and densely rimed plates with simple extensions and crystals with sectorlike branches (hexagons). The best-fit line is for densely rimed columns only.

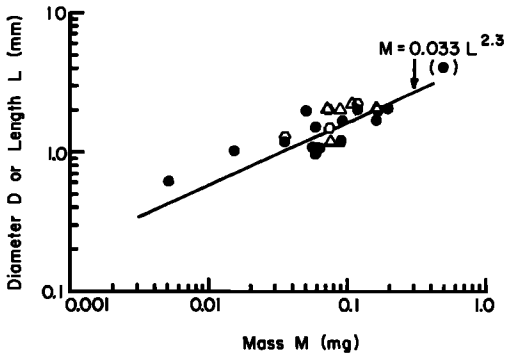

Fig. 15. Diameters or lengths versus masses for densely rimed columns (circles), densely rimed stellars and crystals with broad branches (triangles), and densely rimed plates with simple extensions and crystals with sectorlike branches (hexagons). The best-fit line is for densely rimed columns only.

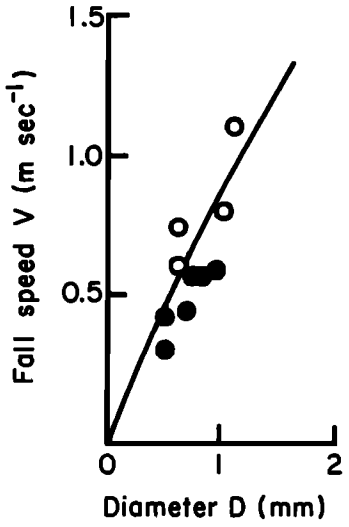

Fig. 16. Fall speeds versus diameters for unrimed side planes. Data from the present study are represented by open circles; data from *Zikmunda and Vali* [1972] are represented by solid circles.

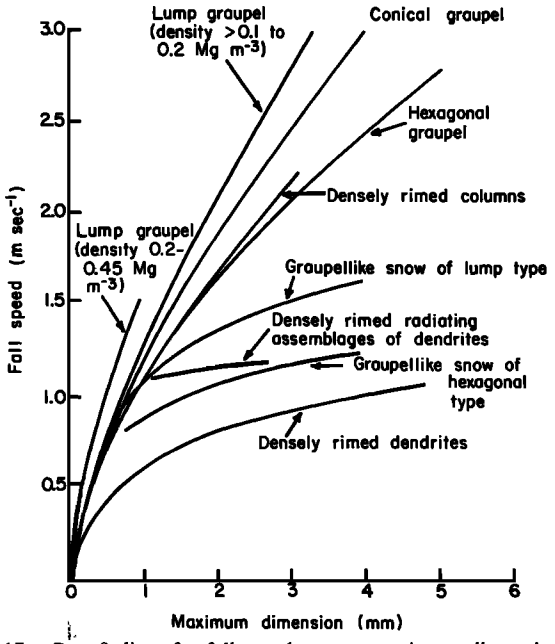

Fig. 17. Best-fit lines for fall speeds versus maximum dimensions of single solid precipitation particles of various types.

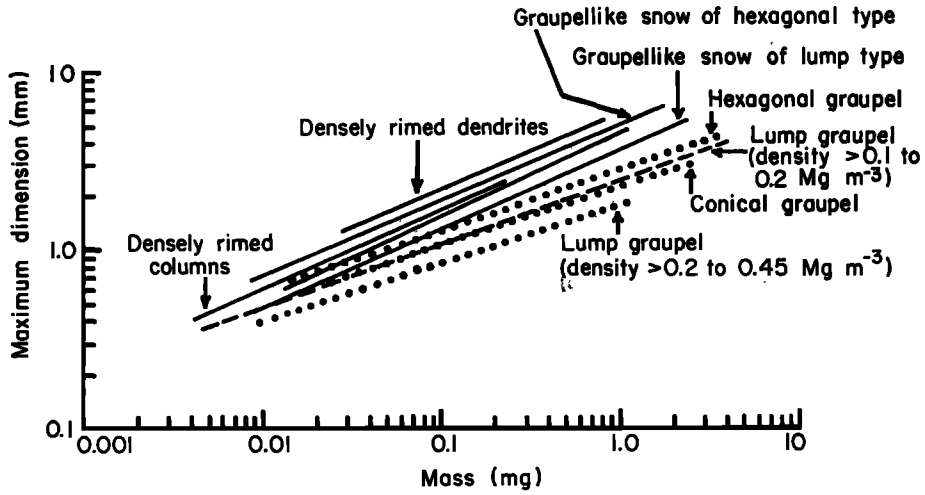

Fig. 18. Best-fit lines for maximum dimensions versus masses for single solid precipitation particles of various types.

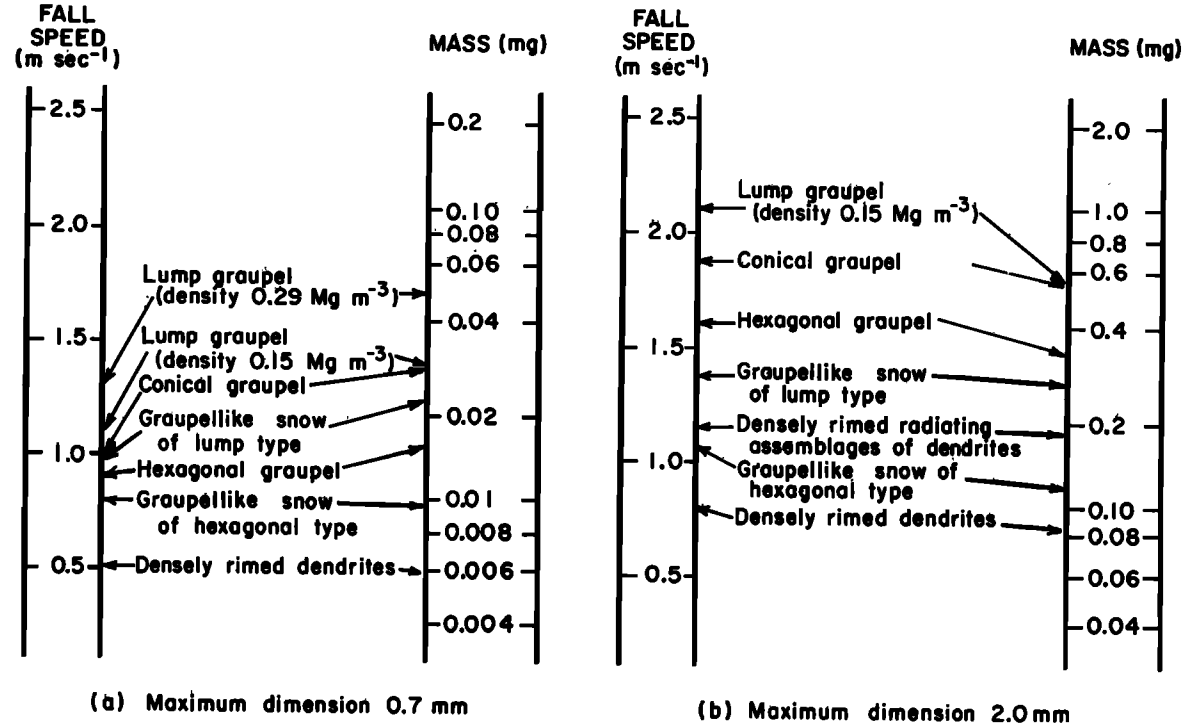

Fig. 19. Order of single solid precipitation particles of various types by fall speed and mass for maximum dimensions of 0.7 and 2.0 mm.

the denser the graupel, the higher its fall speed for a given diameter. Figure 6 shows the mass of graupel as a function of diameter for the three density ranges.

The density of lump graupel against its diameter is shown in Figure 7, where it can be seen that there is a tendency for the density to decrease with increasing size. However, the smaller graupel shows much larger fluctuations in density. The lump graupel collected by *Zikmunda and Vali* [1972] had densities from 0.7 to 0.45 Mg m^{-3} for diameters of 0.5–1.0 mm and from 0.45 to 0.25 Mg m^{-3} for diameters of 1.0–2.0 mm. These densities are about 0.2–0.3 Mg m^{-3} greater than our values. Other workers [*Nakaya and Terada*, 1935; *Magono*, 1954; *List*, 1958] have reported graupel densities from 0.13 to 0.7 Mg m^{-3}. These various values of density probably reflect real differences in the types of graupel sampled rather than experimental errors.

Hexagonal and conical graupel (Figures 2b and 2c). Figures 8 and 9 contain our experimental data for hexagonal and conical graupel. It can be seen that the fall speeds and masses of conical graupel are generally greater than those of hexagonal graupel of comparable dimensions.

Graupellike snow of hexagonal and lump types (Figures 2d and 2e). Our experimental data for these two types of precipitation particle are shown in Figures 10 and 11.

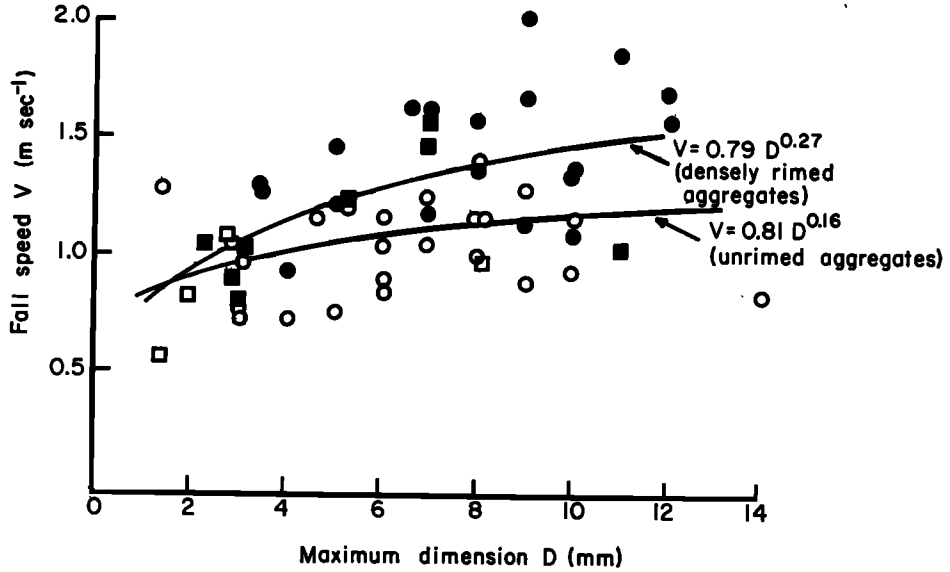

Fig. 20. Fall speeds versus maximum dimensions for unrimed aggregates of radiating assemblages of dendrites (open circles), densely rimed aggregates of radiating assemblages of dendrites (solid circles), unrimed aggregates of dendrites (open squares), and densely rimed aggregates of dendrites (solid squares).

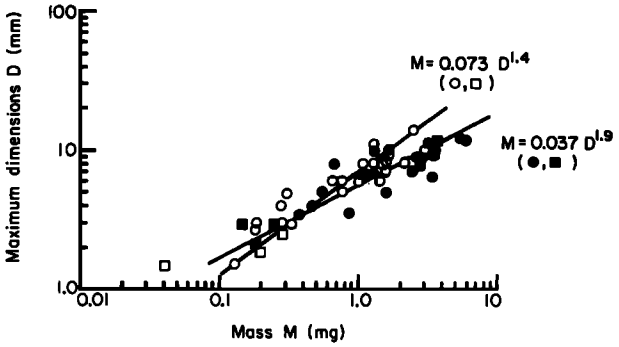

Fig. 21. Maximum dimensions versus masses for unrimed aggregates of radiating assemblages of dendrites (open circles), densely rimed aggregates of radiating assemblages of dendrites (solid circles), unrimed aggregates of dendrites (open squares), and densely rimed aggregates of dendrites (solid squares).

Graupellike snow of lump type, being more massive than graupellike snow of hexagonal type of comparable dimensions, generally has the greater fall speed.

Unrimed and densely rimed radiating assemblages of dendrites and densely rimed dendrites (Figures 2f, 2g, and 2h). The measured fall speeds of these three types of particle are shown in Figure 12. Since we obtained only three datum points for unrimed radiating assemblages of dendrites, a best-fit line is not shown for these crystals. However, in Figure 12 we have plotted relationships between the fall speeds and the diameters of unrimed radiating assemblages of dendrites and unrimed dendrites (Figure 2*i*) given by *Brown* [1970] and *Zikmunda and Vali* [1972]. Comparison of these curves with our results shows that for both radiating assemblages of dendrites and dendrites, dense riming increases the fall speeds by a factor of 1.5–2.0. The masses of the particles are shown in Figure 13.

Densely rimed columns (Figure 2j). Our experimental observations on the fall speeds and masses of densely rimed columns of various lengths are shown in Figures 14 and 15. The ratio of the lengths to the widths of the columns studied

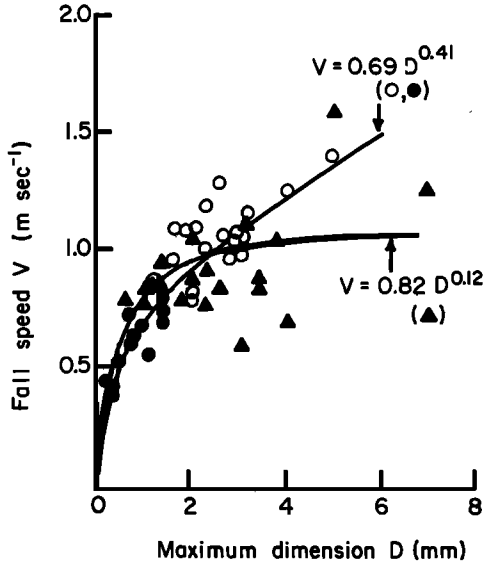

Fig. 22. Fall speeds versus maximum dimensions for unrimed aggregates of side planes, columns, and bullets (open circles); unrimed aggregates of assemblages of plates, side planes, columns, and bullets (solid circles) [*Zikmunda and Vali*, 1972]; and aggregates of unrimed side planes (triangles).

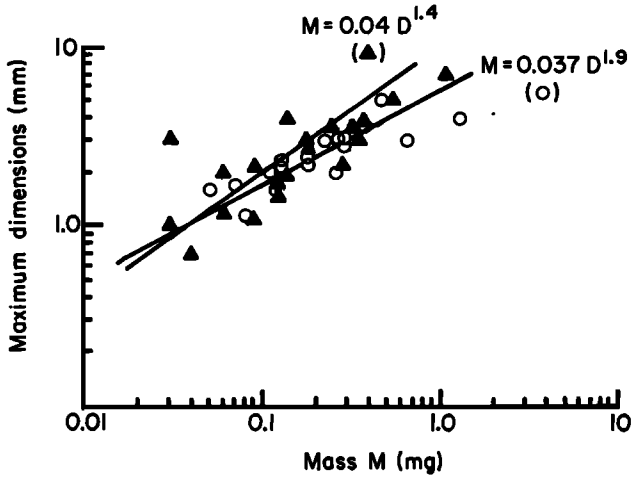

Fig. 23. Maximum dimensions versus masses for aggregates of unrimed side planes (triangles) and for unrimed aggregates of side planes, columns, and bullets (circles).

varied from 1.3 to 2.0, and their densities varied from 0.02 to 0.27 Mg m^{-3}; the density of a densely rimed column appeared to be independent of its length. *Zikmunda and Vali* [1972] reported densities for densely rimed columns in the range 0.2–0.5 Mg m^{-3}; however, the average ratio of the lengths to widths of their columns was 6.6.

Densely rimed plates with simple extensions and crystals with sectorlike branches and densely rimed stellars and crystals with broad branches (Figures 2k, 2l, 2m, and 2n). There were insufficient data to derive reliable best-fit expressions for these particles. The few measurements obtained are shown in Figures 14 and 15.

Unrimed side planes (Figure 2o). The present study yielded only four measurements of the fall speeds of unrimed side planes. These are shown in Figure 16, together with six datum points obtained by *Zikmunda* [1972] and the best-fit line through all 10 points.

Comparison of Data for Single Precipitation Particles

In this section we compare our results for the fall speeds and masses of different types of single precipitation particles in order to demonstrate the effects of riming.

Figures 17 and 18 contain our best-fit lines for the fall speeds and masses of different types of single precipitation particles as a function of their maximum dimensions. It can be seen from Figure 17 that the fall speed of graupel increases with size much more rapidly than the fall speeds of graupellike snow or the densely rimed single particles. The mass of graupel also increases more rapidly with increasing size than the masses of other particles (Figure 18).

The effect of riming on both the fall speed and the mass of a particle of a given size is demonstrated in Figure 19. It can be seen that when a particle passes from densely rimed dendrites through graupellike snow, hexagonal graupel, and conical graupel to lump graupel, the maximum dimension remaining constant, both the fall speed and the mass increase so that the 'rank' of a particle by fall speed is the same as its rank by mass. Note that at a maximum dimension of 2 mm, hexagonal graupel falls faster than graupellike snow of lump type, but at 0.7 mm the reverse is true. Apparently, at diameters less than 1.0 mm, graupellike snow of lump type becomes similar in type to lump graupel, whereas hexagonal graupel approaches graupellike snow of hexagonal type.

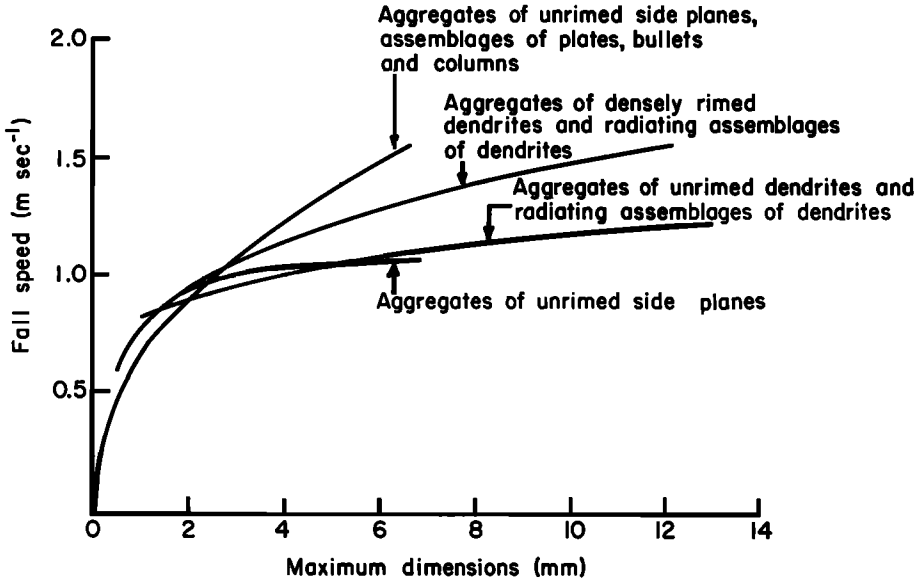

Fig. 24. Best-fit curves for fall speeds versus maximum dimensions for aggregates of various types.

EXPERIMENTAL DATA FOR AGGREGATES

We describe now our experimental data for aggregates of different types of crystals.

Aggregates of unrimed and densely rimed dendrites and radiating assemblages of dendrites (Figures 2p and 2q). The fall speeds and masses of these particles are shown in Figures 20 and 21. Radiating assemblages of dendrites and dendrites have been combined in determining the best-fit curves, so that only two curves are shown on each diagram, one for unrimed aggregates and the other for densely rimed aggregates of these crystals. The densely rimed aggregates are generally more massive and fall faster than the unrimed aggregates of the same size. The densely rimed aggregates have fall speeds about 1.3 times greater than the fall speeds of unrimed aggregates of comparable size, in comparison with single snow particles for which the fall speed increases by a factor of about 2.0 when the particles pass from unrimed to densely rimed particles.

Aggregates of unrimed side planes. Results for these particles are shown in Figures 22 and 23.

Unrimed aggregates of radiating assemblages of plates, side planes, columns, and bullets and unrimed aggregates of side planes (Figures 2r, 2s, 2t, 2u, and 2v). We obtained fall speeds and mass data for particles of this type with maximum dimensions in the range 1.0–5.0 mm (Figures 22 and 23). In obtaining the best-fit line for the fall speeds (Figure 22), we combined our data with those obtained by *Zikmunda* [1972], which covered maximum dimensions from about 0.2 to 1.4 mm. It can be seen in Figure 22 that aggregates of unrimed side planes tend to fall somewhat more slowly than aggregates that include crystals such as bullets and columns, and the latter are somewhat heavier (Figure 23). Apparently, bullets and columns, being more compact crystals than side planes, pack closer together in an aggregate.

COMPARISON OF DATA FOR AGGREGATES

The best-fit curves for the fall speeds and masses of various types of aggregates as a function of their maximum dimensions are shown for comparison in Figures 24 and 25. It is of interest to note that the masses of aggregates of unrimed side planes, bullets, and columns fall on the same line as those of aggregates of densely rimed dendrites and radiating assemblages of dendrites. Also, the slopes of the mass-maximum dimension lines for aggregates of unrimed side planes and aggregates of unrimed dendrites and of radiating assemblages of dendrites are the same. The increase in mass with increasing dimensions is greater for aggregates that are densely rimed or that contain bullets and columns than it is for unrimed aggregates of side planes, dendrites, and radiating assemblages of dendrites.

Aggregates of two sizes are ranked by their fall speeds and masses in Figure 26; it can be seen that the order of rank by fall speed is generally the same as that by mass.

COMPARISON OF FALL SPEEDS OF AGGREGATES WITH THEIR COMPONENT PARTICLES

Shown in Figure 27 are the ranges of fall speeds and maximum dimensions for several different types of aggregates and their component crystals. All the data are from the present study except those for unrimed dendrites, which are from *Brown* [1970], and unrimed radiating assemblages of dendrites, which are from *Zikmunda* [1972]. It can be seen that an

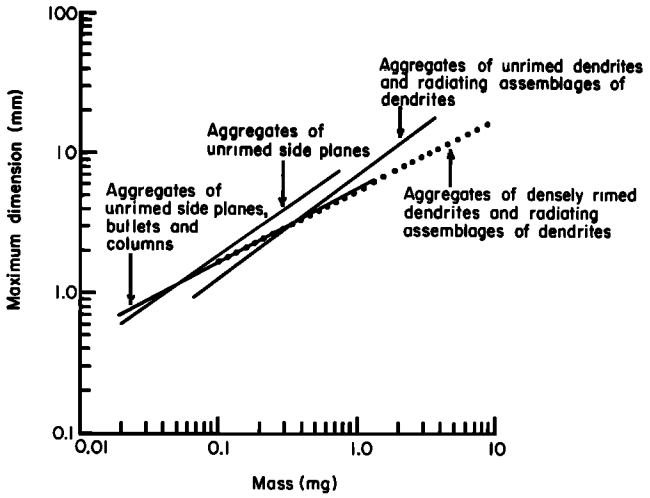

Fig. 25. Best-fit curves for maximum dimensions versus masses of aggregates of various types.

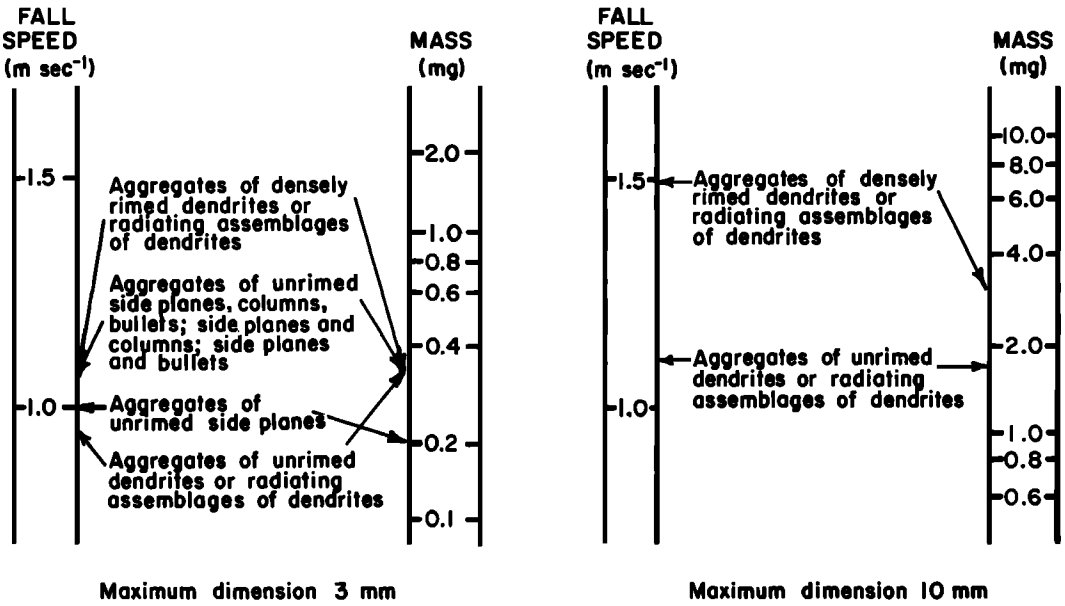

Fig. 26. Order of aggregates of various types by fall speed and mass for maximum dimensions of 3 and 10 mm.

aggregate generally falls faster than its component crystals. It appears that aggregates of unrimed dendrites and radiating assemblages of dendrites might be capable of growing more readily than the other aggregates studied, since these aggregates and their component crystals have a greater difference in fall speed than the other aggregates and their component crystals.

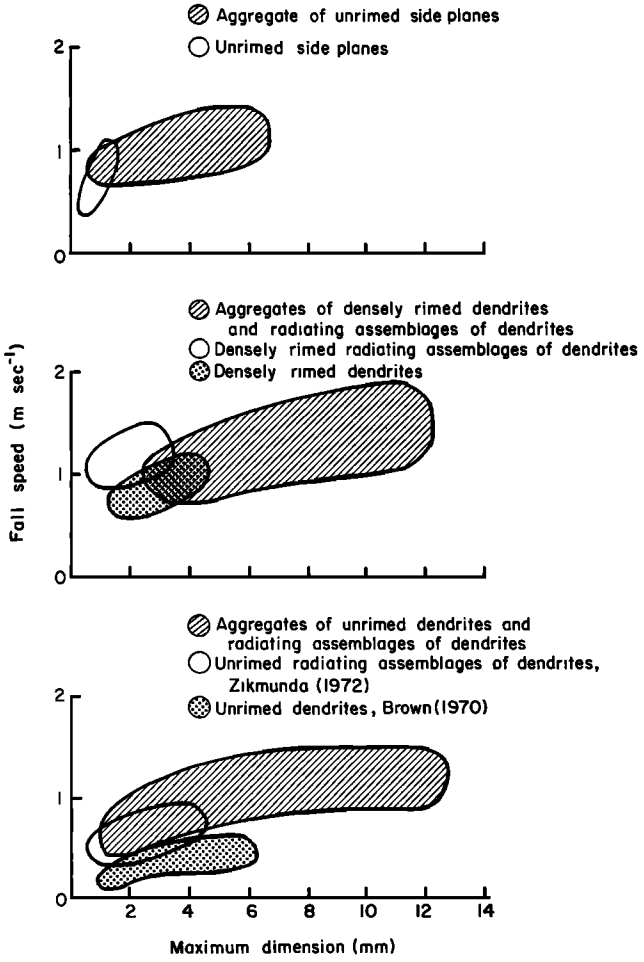

Fig. 27. Range of fall speeds and maximum dimensions for aggregates and their component particles.

Comparison With Previous Observations

In this section we compare our measurements of the fall speeds and masses of solid precipitation particles with those of other workers who have obtained a comparable number of datum points on any of the particles that we studied. In comparing best-fit curves, allowance must be made when different mathematical expressions have been fitted to experimental data. As an example, Figure 28 shows *Zikmunda and Vali*'s [1972] experimental results for conical graupel, together with

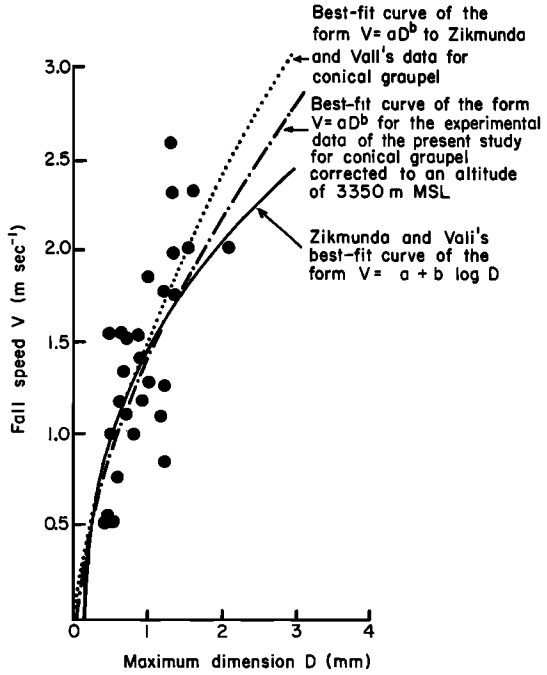

Fig. 28. Two best-fit lines to the experimental data of *Zikmunda and Vali* [1972] for fall speed versus maximum dimension of conical graupel and a best-fit line to the present data for conical graupel.

their best-fit curve, which is of the form $V = a + b \log D$. Also shown in Figure 28 is a best-fit curve of the form $V = aD^b$ to Zikmunda and Vali's data and the best-fit curve of the form $V = aD^b$ to our own experimental data for conical graupel (corrected to the altitude of 3350 m msl, at which Zikmunda and Vali made their measurements). It can be seen that a curve of the form $V = aD^b$ can be fitted more closely to the data than a curve of the form $V = a + b \log D$ and that the best-fit curve to our data differs only slightly from a best-fit curve of the form $V = aD^b$ to Zikmunda and Vali's data.

Our best-fit curves for the fall speeds and masses of solid precipitation particles are compared with the results of other workers in Figures 29 and 30. For the fall speeds of densely rimed columns our best-fit curve appears to agree well with the measurements of Zikmunda and Vali (Figure 29*a*). Note, however, that the rimed columns studied by Zikmunda and Vali had densities about 0.25 Mg m^{-3} greater than those on which we obtained measurements. Zikmunda and Vali give a best-fit line of the form $V = a + b \log D$ for the fall speed as a function of maximum dimension D for graupellike snow of

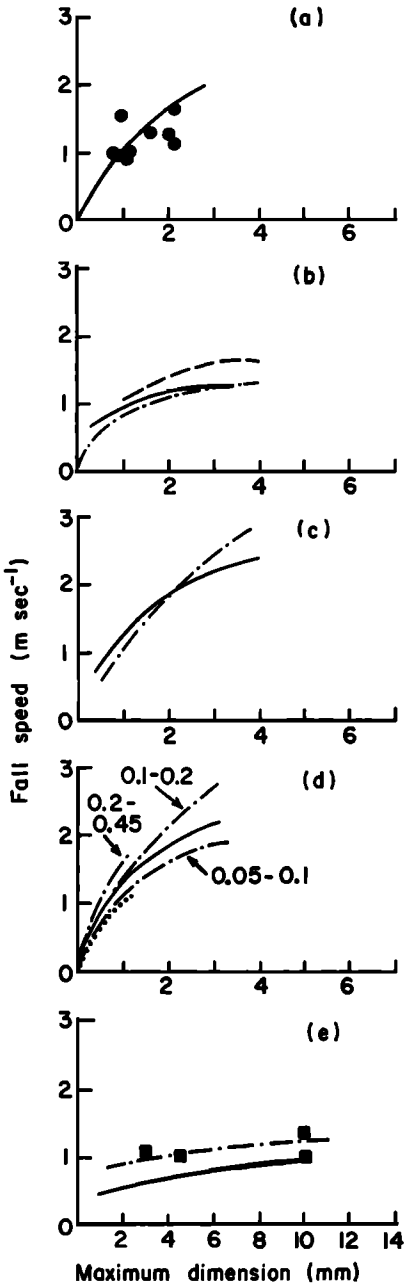

Fig. 29. Comparison of the present results on fall speeds versus maximum dimensions of solid precipitation particles with those of other workers. (*a*) Experimental data for densely rimed columns from *Zikmunda and Vali* [1972] (circles) and best-fit curve for similar particles from the present study (solid line). (*b*) Best-fit curves for graupellike snow of hexagonal and lump type combined from Zikmunda and Vali (solid line), graupellike snow of lump type (broken line) and graupellike snow of hexagonal type (dash-dot line) from the present study. (*c*) Best-fit curves for hexagonal graupel from Zikmunda and Vali (solid line) and from the present study (dash-dot line). (*d*) Best-fit curves for lump graupel from Zikmunda and Vali (solid line), *Bashkirova and Pershina* [1964] (dotted line), and the present study (dash-dot line), the range of densities in megagrams per cubic meter being indicated. (*e*) Experimental data for aggregates of dendrites or dendrites and plate forms from *Jiusto and Bosworth* [1971] (squares) and best-fit curves for aggregates of unrimed dendrites and radiating assemblages of dendrites from *Zikmunda* [1972] (solid line) and the present study (dash-dot line).

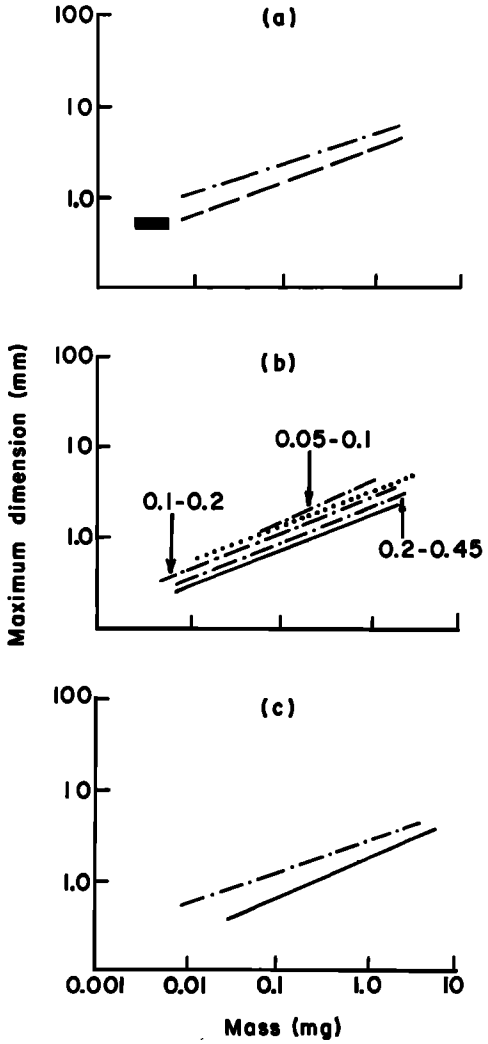

Fig. 30. Comparison of present results on mass versus maximum dimensions of solid precipitation particles with those of other workers. (*a*) Experimental data of *Bashkirova and Pershina* [1964] (bar) for heavily rimed hexagonal snow particles and best-fit curves for graupellike snow of hexagonal type (dash-dot line) and hexagonal graupel (broken line) from the present study. (*b*) Best-fit curve for lump graupel from *Zikmunda and Vali* [1972] (solid line), Bashkirova and Pershina (dotted line), and the present study (dash-dot line), the range of densities in megagrams per cubic meter being indicated. (*c*) Best-fit curve for conical graupel from *Zikmunda and Vali* [1972] (solid line) and the present study (dash-dot line).

hexagonal type and lump type combined; this curve is shown in Figure 29*b*, where it can be seen to agree reasonably well with our best-fit curves (of the form $V = aD^b$) for these two types of particle considered separately. Similarly, their best-fit curve for hexagonal graupel agrees reasonably well with ours considering the different mathematical expressions that were fitted to the data (Figure 29*c*). Our mass–maximum dimension curves for graupellike snow of hexagonal type and hexagonal graupel are compared in Figure 30*a* with some results for 'strongly rimed hexagonal snow particles' obtained by *Bashkirova and Pershina* [1964]. Results for the fall speeds and masses of lump graupel are compared in Figures 29*d* and 30*b* and are seen to be reasonably good. Our best-fit line for the fall speed of conical graupel has already been compared with the data obtained by Zikmunda and Vali (Figure 28). The mass-dimension curves for conical graupel are compared in Figure 30*c*, where it can be seen that the masses that we measured were somewhat less than those reported by Zikmunda and Vali for conical graupel of comparable size. This difference is consistent with the fact that the fall speeds of the conical graupel that we investigated were somewhat less on the average than those reported by Zikmunda and Vali (Figure 28). Plotted in Figure 29*e* are best-fit curves for aggregates of unrimed dendrites and radiating assemblages of dendrites from the present study and that of Zikmunda. Our fall speeds are somewhat greater than those of Zikmunda, but our results agree well with measurements on aggregates of dendrites or aggregates of dendrites and plate forms reported by *Jiusto and Bosworth* [1971]. Each of Jiusto and Bosworth's datum points shown in Figure 29*e* represents the average of many measurements.

Although in this paper we have not presented Best numbers, Reynolds numbers, or drag coefficients for solid precipitation particles based on our measurements, these can readily be determined from our size, mass, and fall speed data and compared with theoretical computations and model experiments.

Conclusions

The following general conclusions can be drawn from the measurements of the fall speeds and masses of the solid precipitation particles that we have studied (viz., lump, conical, and hexagonal graupel; graupellike snow of lump type and hexagonal type; densely rimed dendrites, plates with simple extensions, crystals with sectorlike branches, stellars, crystals with broad branches, columns, and radiating assemblages of dendrites; unrimed side planes; aggregates of densely rimed dendrites and radiating assemblages of dendrites; aggregates of unrimed dendrites and radiating assemblages of dendrites, side planes, and radiating assemblages of plates, side planes, bullets, and columns):

1. Fall speeds increase as the maximum dimensions of the particles increase.
2. Fall speeds increase as the mass of the particles increases.
3. A densely rimed particle falls with a speed up to twice as great as the speed of a similar unrimed particle with the same maximum dimension.
4. For a given maximum dimension the fall speed of a particle increases with increasing density.
5. Aggregates generally fall faster than their component crystals.
6. The rank of particles of similar general types based on their degree of riming is generally the same as their rank based on mass or fall speed.
7. Significant differences exist in the fall speeds and masses of aggregates composed of different types of particles even though the particles may have similar degrees of riming.
8. Of interest is the effect that overseeding with artificial ice nuclei or 'dry ice' might have on the fall speeds (and therefore the trajectories) of snow particles if through seeding, riming is eliminated, but the ice particles then aggregate [*Holroyd and Jiusto*, 1971; *Hobbs et al.*, 1973; *Hobbs and Radke*, 1973]. For example, let us consider single snow particles falling originally as hexagonal graupel that are converted to aggregates of unrimed dendrites following seeding. From the results presented in this paper we see that hexagonal graupel between 1 and 4 mm in size has a fall speed from 0.8 to 2.4 m s^{-1}, unrimed dendrites from 1 to 4 mm in size have fall speeds from 0.3 to 0.6 m s^{-1}, and aggregates of unrimed dendrites from 1 to 14 mm in size have fall speeds from 0.5 to 1.4 m s^{-1}. Therefore even though aggregation increases the fall speeds of single unrimed dendrites, the aggregates fall more slowly than the original hexagonal graupel.

Acknowledgments. We thank John Pinnons, Jack Russell, and Charles Robertson for their help during the course of this work. The research was supported by grant GI-31759 from the RANN Division of the National Science Foundation and contract 14-06-D-6999 from the Division of Atmospheric Water Resources Management, Department of the Interior. This is contribution 298, Department of Atmospheric Sciences, University of Washington, Seattle.

References

Bashkirova, T. A., and T. A. Pershina, On the mass of snow crystals and their fall velocity, *Tr. Gl. Geofiz. Observ.*, Engl. Transl., no. 165, 83–100, 1964.

Brown, S. R., Terminal velocities of ice crystals, M.S. thesis, 52 pp., Colo. State Univ., Fort Collins, 1970.

Hobbs, R. V., and L. F. Radke, Redistribution of snowfall across a mountain range by artificial seeding: A case study, *Science, 181,* 1043–1045, 1973.

Hobbs, P. V., R. C. Easter, and A. B. Fraser, A theoretical study of the flow of air and fallout of solid precipitation over mountainous terrain, 2, Microphysics, *J. Atmos. Sci., 30,* 813–823, 1973.

Holroyd, E. W., and J. E. Jiusto, Snowfall from a heavily seeded cloud, *J. Appl. Meteorol., 10,* 266–269, 1971.

Jiusto, J. E., and G. W. Bosworth, Fall velocity of snowflakes, *J. Appl. Meteorol., 10,* 1352–1354, 1971.

Langleben, M. P., The terminal velocity of snowflakes, *Quart. J. Roy. Meteorol. Soc., 80,* 174–181, 1954.

List, R., Kennzeichen atmosphärischer Eispartikel, 1, Teil, *Z. Angew. Math. Phys., 9a,* 180–192, 1958.

Litvinov, I. V., Determination of falling velocity of snow particles, *Izv. Akad. Nauk SSR, Ser. Geofiz.*, Engl. Transl., no. 7, 853–856, 1956.

Magono, E., On the fall velocities of snowflakes, *J. Meteorol., 8,* 199–200, 1951.

Magono, C., On the falling velocities of solid precipitation elements, *Sci. Rep. Yokohama Univ., Sect. 1,* no. 3, 33, 1954.

Magono, C., and C. V. Lee, Meteorological classification of natural snow crystals, *J. Fac. Sci. Hokkaido Univ., Ser. 7, 2,* 321–362, 1966.

Nakaya, U., and T. Terada, Simultaneous observation of the mass, falling velocity and form of snow crystals, *J. Fac. Sci. Hokkaido Univ., Ser. 2, 1,* 191–201, 1935.

Zikmunda, J., Fall velocities of spatial crystals and aggregates, *J. Atmos. Sci., 29,* 1511–1515, 1972.

Zikmunda, J., and B. Vali, Fall patterns and fall velocities of rimed ice crystals, *J. Atmos. Sci., 29,* 1334–1347, 1972.

(Received November 1, 1973;
revised February 11, 1974.)